Coordination changes and auto-hydroxylation of FIH-1: Uncoupled O2-activation in a human hypoxia sensor

ARTICLE *in* JOURNAL OF INORGANIC BIOCHEMISTRY · SEPTEMBER 2008

Impact Factor: 3.44 · DOI: 10.1016/j.jinorgbio.2008.07.018 · Source: PubMed

Published in final edited form as:
J Inorg Biochem. 2008 December ; 102(12): 2120–2129. doi:10.1016/j.jinorgbio.2008.07.018.

Coordination changes and auto-hydroxylation of FIH-1: uncoupled O_2-activation in a human hypoxia sensor

Yuan-Han Chen[1,2], **Lindsay M. Comeaux**[1], **Robert W. Herbst**[1], **Evren Saban**[1], **David C. Kennedy**[1], **Michael J. Maroney**[1,2], and **Michael J. Knapp**[1,2,*]

1*Department of Chemistry, University of Massachusetts, Amherst, MA, 01003*

2*Program in Molecular Cellular Biology, University of Massachusetts, Amherst, MA, 01003*

Abstract

Hypoxia sensing is the generic term for pO_2-sensing in humans and other higher organisms. These cellular responses to pO_2 are largely controlled by enzymes that belong to the Fe(II) α-ketoglutarate (αKG) dependent dioxygenase superfamily, including the human enzyme called the Factor Inhibiting HIF (FIH-1), which couples O_2-activation to the hydroxylation of the Hypoxia Inducible Factor α (HIFα). Uncoupled O_2-activation by human FIH-1 was studied by exposing the resting form of FIH-1, (αKG+Fe)FIH-1, to air in the absence of HIFα. Uncoupling lead to two distinct enzyme oxidations, one a purple chromophore (λ_{max} = 583 nm) arising from enzyme auto-hydroxylation of Trp^{296}, forming an Fe(III)–O–Trp^{296} chromophore (Y.-H. Chen, L. M. Comeaux, S. J. Eyles, M. J. Knapp, Chem. Commun. (2008) DOI:10.1039/B809099H); the other a yellow chromophore due to Fe(III) in the active site, which under some conditions also contained variable levels of an oxygenated surface residue, (oxo)Met^{275}. The kinetics of purple FIH-1 formation were independent of Fe(II) and αKG concentrations, however product yield was saturable with increasing [αKG] and required excess Fe (II). Yellow FIH-1 was formed from (succinate+Fe)FIH-1, or by glycerol addition to (αKG+Fe) FIH-1, suggesting that glycerol could intercept the active oxidant from the FIH-1 active site and prevent hydroxylation. Both purple and yellow FIH-1 contained high-spin, rhombic Fe(III) centers, as shown by low temperature EPR. XAS indicated distorted octahedral Fe(III) geometries, with subtle differences in inner-shell ligands for yellow and purple FIH-1. EPR of Co(II)-substituted FIH-1, (αKG+Co)FIH-1, indicated a mixture of 5-coordinate and 6-coordinate enzyme forms, suggesting that resting FIH-1 can readily undergo uncoupled O_2-activation by loss of an H_2O ligand from the metal center.

Keywords

HIF; hypoxia; non-heme iron; α-ketoglutarate; protein oxidation; factor inhibiting HIF; asparaginyl hydroxylase

Introduction

Hypoxia sensing is crucial for tissue development and angiogenesis in most animals, as this is the signal that pO_2 is below the ideal set-point. Humans and many other higher organisms

*Corresponding author: E-mail: mknapp@chem.umass.edu; Phone: 413-545-4001; Fax: 413-545-4490.

utilize a complex system for sensing oxygen which relies upon the hydroxylation of specific residues on a transcription factor called the hypoxia inducible factor (HIF), a heterodimer consisting of the O_2-sensitive HIFα subunit and the constitutive HIFβ subunit (also known as the Aryl Hydrocarbon Nuclear Translocator). HIF promotes the expression of genes involved in anaerobic metabolism, angiogenesis, and iron uptake in response to pO_2; for reviews, see [1–4]. The key players regulating HIF are the human enzymes HIF-asparaginyl hydroxylase (previously identified as factor inhibiting HIF, FIH-1), and the HIF-prolyl hydroxylases, each of which hydroxylate residues on HIFα [5–7].

The HIF hydroxylases are members of the large and diverse superfamily of non-heme Fe(II), α—ketoglutarate dependent oxygenases. Enzymes of this class activate O_2 via the oxidative decarboxylation of α–ketoglutarate (αKG), leading to an Fe(IV)=O intermediate which oxidizes or oxygenates the primary substrate (Scheme 1) [8–10]. The Fe(II) in resting enzyme is approximately octahedral, coordinated by a His_2Asp/Glu facial triad, bidentate αKG, and an axial H_2O ligand. A key step in the consensus mechanism is the controlled loss of the axial H_2O, which ensures coupling between the formation of the Fe(IV)=O and substrate hydroxylation [8]. In this step, the axial H_2O is released when prime substrate binds, forming a 5-coordinate Fe(II) center which can bind and activate O_2 [11,12]. Consequently, the controlled changes in the coordination geometry of Fe(II) is a key determinant of enzyme fidelity.

Nevertheless, many enzymes from the αKG oxygenase superfamily rapidly inactivate due to metal oxidation or auto-hydroxylation. Spectroscopic methods indicate that the coordination changes described above are not absolute, and that the resting form of several enzymes contain Fe(II) in a mixture of 5C and 6C forms [13,14], suggesting that O_2 activation may occur prior to binding prime substrate. This is borne out by the need for ascorbate in turnover assays to regenerate Fe(II) from Fe(III) for maximal enzyme activity, an effect related to the dietary need of vitamin C to prevent scurvy. There are also several examples of auto-hydroxylation or auto-oxygenation in αKG oxygenases, which frequently lead to inactive enzyme [15–20], In many cases, a new charge-transfer transition appears from the coordination of hydroxylated Tyr or Trp residues to Fe(III) in the active site. In view of the examples of ready inactivation for αKG-oxygenases, it is somewhat surprising that nature would choose such enzymes as oxygen sensors.

The X-ray crystal structure of human FIH-1 indicates that the Fe(II) is 6C in resting enzyme, with a limited hydrogen bonding network [21–23]. Three aromatic residues are within 12 Å of the iron, forming ripe targets for auto-hydroxylation (Figure 1). Recently, we showed that FIH-1 forms a purple Fe(III)-O-Trp chromophore, in which Trp^{296} was auto-hydroxylated [24]. Herein, we test the link between auto-hydroxylation and coordination changes at the metal center, and characterize two different forms of the oxidized human FIH-1 which contain oxygenated residues.

Materials and Methods

Protein expression and purification

The gene for FIH-1 was subcloned from the IMAGE clone 4138066 [25] purchased through the American Type Culture Collection, and FIH-1 protein was expressed similar to literature precedent [26]. Briefly, PCR-amplified fragments of the FIH-1 gene were inserted into a pET28a plasmid (Novagen) via NdeI and BamHI restriction sites with an N-terminal hexa-histidine tag, and the sequence confirmed by DNA sequencing at the Yale/W.M. Keck sequencing center. *E. coli* BL21(DE3) cells were transformed, grown on LB plates, then grown as overnight liquid cultures at 37° C. Fresh LB media was inoculated with the overnight cultures at a 1:500 ratio, and grown at 37° C. His_6-FIH-1 expression was induced by the addition of

IPTG (0.5mM) at OD_{600} between 0.5 – 0.7. Protein was expressed for 5 hours, then the cells harvested by centrifugation and frozen.

Frozen cell paste was suspended in lysis buffer (25 mM Tris, pH 8.00, containing 0.1 mM EDTA, 0.5 mg/ml lysozyme, and 5 μM AEBSF on ice for 1 hour, followed by sonication to lyse the cells. Crude lysate was centrifuged, followed by dialysis with 50 mM Tris buffer pH 8.00 to remove EDTA. Dialysed lysate was clarified with 40 μm membrane, then loaded onto a Ni-NTA His-bind Superflow (Novagen) column (2 × 10 cm) using loading buffer (50 mM NaH_2PO_4, 300 mM NaCl, and 10 mM Imidazole pH 8.00). His_6-FIH-1 was first washed with 15% elution buffer (50 mM NaH_2PO_4, 300 mM NaCl, and 250 mM imidazole pH 8.00), and then eluted with 100% elution buffer. Salt was removed by serial cycles of ultraconcentration and dilution with 50 mM Tris buffer pH 8.00. His_6-FIH-1 was cleaved by thrombin at 4° C for 2 days, and then loaded onto the Ni-column again to separate FIH-1 from uncleaved His_6-FIH-1. The flow-through was concentrated and loaded onto an S200 size exclusion column (1.5 × 100 cm) to purify dimeric FIH-1. Metal-free FIH-1 (Apo FIH-1) was prepared by incubation with 50 mM EDTA at 4° C for 1 day, followed by concentration and buffer exchange (50 mM HEPES pH 7.50), and frozen at −20° C. Protein concentration was determined by A_{280} readings, and referred to on a per monomeric subunit basis. The extinction coefficient for apo FIH-1 was determined (ε_{280} = 48.8 mM^{-1} cm^{-1}) by the method of Gill [27].

Preparation of metal-reconstituted FIH-1

To reconstitute (αKG/succ+Fe)FIH-1, anaerobic stock solutions of apo FIH-1 (1.00 mM), $FeSO_4$•$7H_2O$ (10 mM), and αKG (10 mM) or succinate (10 mM) in 50 mM HEPES pH 7.50 were prepared and kept in an anaerobic chamber. Stock FIH-1 (10 μl) was diluted into 100 μl by HEPES buffer with varied amounts of Fe(II) and μKG or succinate, which were added at 30 min. intervals. The mixture was incubated for 30 min. prior to measurements.

To reconstitute (αKG+Co)FIH-1, aerobic apo FIH-1 stock (1.00 mM) was diluted with 50 mM HEPES pH 7.50 to a final concentration of 100μM. Stock solutions of $CoCl_2$ (10 mM $CoCl_2$, 50 mM HEPES pH 7.50) and αKG (10 mM αKG/50 mM HEPES pH 7.50) were added into the protein solution at 30 min. intervals, to final concentrations of 100 μM, and 500 μM, respectively. After 30 min. incubation, the mixture was concentrated and buffer exchanged with 10 kDa cut-off microcon concentrators (Millipore), and the final FIH-1 concentration was determined by A_{280}.

Auto-oxidation kinetics

An Agilent HP 8453 diode-array UV-Vis spectrometer was used, with masked cuvettes. Apo FIH-1 and all other reagent stocks were prepared, degassed, and then manipulated in an anaerobic chamber. Experiments were performed in 50 mM HEPES, pH 7.50 at room temperature (20 – 23°C) unless noted otherwise. Rapid oxygenation was achieved by addition of aerobic buffer to anaerobic FIH-1 samples within a sealed cuvette. Slow oxygenation was achieved by removal of the cap from a sealed cuvette containing anaerobic FIH-1 samples.

EPR Spectroscopy

EPR spectra were collected in 3 mm quartz tubes using a Bruker ELEXSYS E-500 X-band spectrometer, with a helium flow cryostat. Purple FIH-1 was prepared by slow oxygenation of (αKG+Fe)FIH-1; yellow FIH-1 was similarly prepared from an FIH-1 sample that only formed the yellow chromophore. Spectral simulations used standard spin Hamiltonians [28] within XSophe software package, version 1.1.4 [29].

X-ray spectroscopy

XAS data was collected as previously described on beamline 9-3 at Stanford Synchrotron Radiation Laboraotry (SSRL) [30]. The same FIH-1 samples used for EPR experiments (3 mM FIH-1) were syringed into polycarbonate holders closed with kapton tape, frozen in liquid nitrogen, and analyzed near 10 K using a liquid He cryostat. The ring conditions for data collection were 3 GeV and 80–100 mA. Beam line optics consisted of a Si(220) double-crystal monochromator and two rhodium coated mirrors, a flat mirror before the monochromator for harmonic rejection and vertical collimation, and a second toroidal mirror after the monochromator for focusing. X-ray fluorescence was collected using a 30-element Ge detector (Canberra). Scattering was minimized by placing a set of Soller slits with a Z-1 element filter between the sample chamber and the detector. X-ray absorption near-edge spectroscopy (XANES) was collected from ±200 eV relative to the Fe edge. Extended X-ray absorption fine structure (EXAFS) was collected to $k = 16$ Å^{-1}. The X-ray energy for the K-edge of Fe was internally calibrated to 7111.2 eV using transmission data from a Fe foil. The data shown is the average of 4 – 8 scans and was analyzed using the EXAFS123 (XANES) and SIXPACK (EXAFS) software package [31] with phase and amplitude parameters obtained from prior FEFF8 calculations [32].

Mass spectrometry

Tryptic digests of FIH-1 (10 μM) were frozen in 30 μL aliquots, thawed immediately prior to analysis, and injected in 30 μL volumes for LC-MS/MS analysis. Chromatography was carried out with an Agilent 1100 HPLC connected to a 150 × 2.1 mm PLRP-S column (Polymer Laboratories, Amherst, MA) with 300 Å pore size and 3 μm particle size, using a H_2O/CH_3CN (0.1% formic acid) gradient at a flow rate of 200 μL/min. Preliminary work utilized a Bruker Esquire ion trap mass spectrometer, to identify tryptic peptide masses. High-resolution and MS/MS analysis was carried out using an Applied Biosystems QStar time-of-flight (TOF) mass spectrometer,

Results and Discussion

Coordination geometry of (αKG+Fe)FIH-1 is 5C/6C

The coordination geometry of the metal center in (αKG+Fe)FIH-1 was tested by EPR spectroscopy of the Co(II)-substituted enzyme, (Co)FIH-1. As the electronic environment of Co(II) changes due to coordination geometry and site symmetry, the EPR lineshape is a sensitive reporter of the local environment in Co(II)-substituted metalloenzymes [33–36]. Co (II) in biologically relevant, pseudo-octahedral environments typically has a large zero-field splitting ($DS_z^2 \gg g\beta BS$), such that only the lowest $M_S = |\pm 1/2>$ Kramers doublet is observable. As a consequence, the most useful information from Co(II) EPR is the rhombicity, *E/D*, as this reports on the electronic site symmetry. Due to the strong crystal-field preference for axial electronic symmetries in Co(II), bonding to solvent-derived ligands will adapt so that Co(II) can adopt axial electronic symmetry. On the other hand, the geometric constraints of the protein fold frequently leads to rhombic site symmetry when only protein-derived ligands are present. As a result, a reduced value of *E/D* for Co(II) is an indicator for the presence of solvent-derived ligands. In the case of (αKG+Co)FIH-1, a resting enzyme with three protein-derived ligands, a bidentate αKG, and a H_2O would be 6C, and expected to adopt axial electronic symmetry. Should the H_2O ligand be absent, the resultant 5C center would likely exhibit rhombic electronic symmetry.

(αKG+Co)FIH-1 was frozen in an EPR tube over liquid nitrogen, then inserted into a cooled (~ 20K) helium flow cryostat. X-band EPR spectra were collected over the range 4 – 20 K, with noticeably better signal intensity observed at 9.5 – 11 K. The EPR spectra of each (αKG +Co)FIH-1 sample contained at least two different signals (Figure 2). A broad axial signal near

g_{eff} = 4 was apparent, as expected for Co(II) with axial electronic symmetry. Each sample also exhibited fine structure due to Co hyperfine splitting (A_{obs} ~ 80 G), centered near g_{eff} = 6; these hyperfine lines must arise from a Co(II) in a rhombic electronic environment, as they are were not centered on the g_{eff} = 4 feature. Sample and instrumentation conditions were varied in an attempt to isolate 'pure' signals from each of the Co(II) species; these included sample pH (6, 7, 10), the addition of a glassing agent, and acquisition parameters (4.2 – 20 K, 0.02 – 20 mW power). Standard conditions for optimal signal in the absence of saturation were T = 10 ± 1 K, with microwave power of 0.2 – 2.0 mW.

While both Co(II) sites were observed under all conditions attempted, the low pH sample with glassing agent (50% glycerol, 10 mM Bis-Tris, pH 6.0) exhibited the most prominent rhombic signal, whereas the high pH sample (10 mM CHES, pH 10.0) acquired at 0.2 mW power exhibited the smallest intensity for the rhombic species. This high pH sample could be simulated using g_{iso} = 2.35, E/D = 0.10[†] within the standard spin Hamiltonian:

$\widehat{H}=\beta B_0 g S + D[S_z^2 - {}^1\!/_3\, S(S+1) + {}^E\!/_D\,(S_x^2 - S_y^2)] + SAI$, where β is the Bohr magneton, B_0 the applied magnetic field, S the spin operator, D the axial zero-field splitting, E/D the rhombicity of the zero-field splitting, A the hyperfine coupling constant for ^{59}Co, and I the nuclear spin of ^{59}Co. These electronic parameters were reasonable for axial Co(II), in which the value for $|D|$ was much larger than the Zeeman splitting [33,36]. This likely arose from the 6C center which contained one H_2O ligand. Spectral subtraction of the high pH signal from the low pH signal produced a difference spectrum that was clearly a rhombic signal, albeit with some lineshape distortion. This difference spectrum was simulated with $g_{x,y}$ = 2.60, g_z = 2.30, E/D = 0.23, A_{iso} = 7.7 mT, and while the difference spectrum is distorted, the key features expected for rhombic Co(II) are clearly present, in particular the resolved hyperfine splitting centered at g_{eff} = 6. This rhombic signal was attributed to a 5C species which likely lacks the H_2O ligand.

The EPR spectra indicated that the resting form of (αKG+Co)FIH-1 was a mixture of axial and rhombic Co(II) sites, which we interpret to indicate the presence of a 5C site lacking the H_2O ligand. As the Irving-Williams series predicts that Co(II) will bind a common ligand shell more tightly than Fe(II) [37–39], this suggests that the resting form of Fe-constituted FIH-1 will also exist in an equilibrium of 5C and 6C forms – in fact, the Fe(II) may favor 5C to an even greater extent than the Co(II). Such a weakened axial H_2O ligand has been observed in the resting form of other αKG oxygenases, such as TauD and CytC3 [14], where the 6C resting (αKG+Fe) species exhibit significant distortions due to an elongated metal-ligand bond. Within the context of the consensus mechanism for αKG oxygenases, loss of the H_2O-ligand makes the enzyme ready for O_2-activation [8,12,40]; when H_2O-loss is uncoupled from the binding of prime substrate, uncoupled oxidation can occur, as seen in select bacterial members of the αKG oxygenase superfamily [8]. This suggests that FIH-1 may uncouple O_2-activation from HIFα under certain conditions, leading to enzyme oxidation at either the metal center or at the protein structure.

FIH-1 uncouples O_2-activation

Reconstituting FIH-1 with Fe(II) and αKG under anaerobic conditions forms (αKG+Fe)FIH-1, which exhibits a faint chromophore with λ_{max} = 500 nm (Figure 3). This optical feature has been assigned as a charge transfer transition between αKG and Fe(II) in other αKG oxygenases [12], indicating that resting FIH-1 in solution binds αKG in a bidentate fashion as found crystallographically [21]. This MLCT has a comparable extinction coefficient (ε_{500} = 0.24 mM^{-1} cm^{-1}), but is slightly higher in energy than, those found for TauD [41], TfdA [17], and

[†] D was fixed arbitrarily at 50 cm^{-1} and A was fixed at zero.

CS2 [42], suggesting that FIH-1 contains either a stronger Fe-αKG bond, or a more Lewis-acidic Fe(II) center, than in these other oxygenases.

(αKG+Fe)FIH-1 auto-hydroxylated once the cuvette was opened to air, generating a purple Fe(III)-O-Trp chromophore having λ_{max} = 583nm ($\varepsilon_{583} = 3 \times 10^3\ M^{-1}\ cm^{-1}$, assuming full conversion of apo FIH-1) [24]. This closely resembled the charge-transfer band from Fe(III)-O-Trp centers, formed upon auto-oxidation in two bacterial members of the αKG oxygenase superfamily: TfdA (λ_{max} = 580 nm) [17] and AlkB (λ_{max} = 595 nm) [15], which result from O_2-activation in the absence of the prime substrate. The yield of purple FIH-1 varied with different oxygenation procedures (Figure 4), however the initial rate was very slow under all tested conditions ($v_0 = 10^{-8}\ M\ s^{-1}$),‡ as expected for uncoupled O_2-activation. When 100 μL of anaerobically prepared (αKG+Fe)FIH-1 (500 μM in 50 mM HEPES, pH 7.50, 2.5 mM $FeSO_4$, 2.5 mM αKG) was slowly oxygenated by adding 400 μL anaerobic buffer, then allowing air to diffuse into the opened cuvette, an initial lag phase was observed, followed by a large ΔA_{583}. Conversely, when 100 μL of anaerobically prepared (αKG+Fe)FIH-1 was diluted with aerobic buffer (400 μL) then opened to air, a modest increase in A_{583} followed. We attribute the lag phase to air diffusing into the cuvette, as it was not observed under rapid oxygenation conditions. As the rate of oxygenation affected the yield of purple chromophore, this suggested that rapid introduction of air likely depleted the available pool of Fe(II) in solution, which both reduced yield and slowed the rate of auto-hydroxylation.

The kinetics of auto-hydroxylation were monitored for their dependence on varied concentrations of Fe(II) and αKG. Auto-oxidation reactions with varied [Fe(II)] were performed by preparing an anaerobic solution of apo FIH-1 (100 μM in 100 μL buffer), αKG (500 μM), and variable $FeSO_4$ (50 – 500 μM), then initiating reaction by adding 100 μL aerobic buffer. Under low [Fe(II)] conditions, very little purple chromophore was produced, suggesting that air oxidation of Fe(II) depleted the pool of available metal. In contrast, at excess [Fe(II)] the rate and yield were high and indistinguishable (Figure 5), indicating that the rate-limiting step occurred after Fe(II) bound to FIH-1, provided that the Fe(II) pool was in excess.

The αKG dependence of auto-hydroxylation was assessed under conditions in which FIH-1 (100 μM, 50 mM HEPES, pH 7.50) was preincubated anaerobically with saturating $FeSO_4$ (500 μM) and variable αKG (50 – 1000 μM), then opened to air (Figure 6). The yield increased in response to [αKG] in a saturable fashion, suggesting that an αKG binding equilibrium preceded the reaction. As the rate of formation was independent of [αKG], a step after αKG binding must be rate-determining. Furthermore, as experiments in which αKG was replaced by succinate did not support purple FIH-1 formation (see below), the purple chromophore is likely formed by a high-valent oxidant within the active site, such as the canonical Fe(IV)=O.

Some preparations of FIH-1 formed a yellow chromophore under auto-hydroxylation conditions, with little or no yield of the Trp-O-Fe(III) species. The yellow color arose from a shoulder in the UV-Vis spectrum 300 – 400 nm, indicating metal-centered oxidation to Fe(III). As the formation of yellow FIH-1 was not uniformly observed, we suspected that trace redox agents introduced during protein purification could redirect oxidation toward iron and away from enzymatic hydroxylation.

To test this model, we assayed auto-hydroxylation in the presence of 1mM NaN_3 or glycerol, as these are preservatives for the dialysis membranes used in protein concentrators. Apo FIH-1 (100 μM) was incubated in 100 μL with αKG (500 μM) and $FeSO_4$ (100 μM) under anaerobic conditions, then 100 μL of aerobic buffer containing either no additive, NaN_3 (2 mM), or glycerol (2 mM) was added to initiate auto-oxidation. While the (αKG+Fe)FIH-1 sample

‡Assuming ε_{583}= 3000 $M^{-1}\ cm^{-1}$ for purple FIH-1

generated purple FIH-1 in the positive control (no additive), as well as a slightly reduced yield in the presence of azide, a resolved absorption peak was not found in the presence of glycerol (Figure 7a). It appeared that 1 mM glycerol almost completely prevented the formation of the purple chromophore, suggesting that this preservative was to blame the variable yield of purple FIH-1 in different FIH-1 preparations.

As auto-hydroxylation was specifically localized to Trp^{296}, it likely results from a non-diffusable oxidant. In analogy with other αKG oxygenases, this implicates a metal-centered oxidant in Trp hydroxylation, such as Fe(IV)=O. The fact that glycerol quenched the auto-hydroxylation reaction suggests that glycerol can reach the active site of FIH-1 and intercept this metal-centered oxidant. Notably, the active site of FIH-1 is relatively solvent exposed in the X-ray crystal structure [21], which is consistent with this proposal.

The appearance of purple FIH-1 required αKG, Fe(II), and O_2, however we wished to test whether this was due to oxidative decarboxylation chemistry. Succinate was used in place of αKG, as both succinate and αKG are anionic ligands with similar chelation modes, but succinate does not undergo oxidative decarboxylation. Apo FIH-1 (100 μM) was pre-incubated with one equivalent of $FeSO_4$, and an excess of organic diacid (500 μM αKG or succinate), then rapidly oxygenated by dilution with an equal volume of oxygenated buffer. Quite different products were formed during the subsequent reaction, as shown by the changes in the UV-Vis spectra (Figure 7b). The HO-Trp was clearly formed in the positive control, but absent from (succ. +Fe)FIH-1. As αKG can undergo oxidative decarboxylation to form the high-valent Fe(IV)=O oxidant found in related enzymes, whereas succinate cannot, this result strongly suggests that HO-Trp formation results from the high-valent oxidant.

Metal Oxidation in Purple and Yellow FIH-1

EPR and X-ray absorption spectroscopy were used to characterize the active-site Fe in purple and yellow FIH-1. EPR spectra collected near 10 K for purple and yellow FIH-1 exhibited signals near g_{eff} = 9 and 4.27, indicating the presence of high-spin Fe(III) (Supplemental material). These signals must come from Fe(III) centers tightly associated with FIH-1, as buffer exchange did not remove these EPR signals, indicating that the cofactor of FIH-1 was oxidized upon air exposure.

The coordination geometries of purple and yellow FIH-1 were measured by Fe X-ray absorption spectroscopy. The edge energy for purple FIH-1 lies at 7124.2 eV compared to the 7125.0 eV edge energy for yellow FIH-1, indicating either that there is a small fraction of reduced iron in yellow FIH-1, or that purple FIH-1 is more Lewis-acidic than yellow FIH-1. Each sample exhibited a $1s \rightarrow 3d$ pre-edge transition in the XANES region near 7113.5 eV, indicating that iron deviated from octahedral symmetry[43] (Figure 8).

The EXAFS of each sample was fit to Fourier-filtered data from 1 to 2.3 $Å^{-1}$ to obtain the best first coordination sphere fit. The best fits are shown in Table 1; Alternative fits and fits used to refine the model are shown in the supporting information. The best fit for the purple FIH-1 sample was for a six-coordinate Fe center with two different scattering distances: 2 N/O scatterers at a shorter distance (1.97 Å) and 4 N/O scatterers at a longer distance (2.11 Å). This was consistent with tighter bonds to the two protein-derived anionic ligands, Asp and Trp-O^{-}, with longer bonds to the two His residues, and the remaining two sites occupied by a combination of H_2O and organic acid (αKG or succinate). The yellow FIH-1 sample fit best to 7 N/O scatterers at the same distance (2.01 Å). It is possible that one of the anticipated carboxylate ligands, either Asp or αKG/succinate, was ordered sufficiently that the non-bonded oxygen contributed to scattering. In fact, the difference between the coordination numbers suggested by XANES (5C, or distorted 6C) and determined by EXAFS (6C or 7C) likely arises from the presence of carboxylate ligands that may adopt a bidentate binding mode. For the

purposes of XANES analysis, the bidentate ligand would reduce the symmetry of the iron site, leading to an increase in the 1s → 3d peak area. The Fourier-filtered spectra of the two samples look very similar, with minor differences at 10 $Å^{-1}$ and beyond (Figure 8). These differences most likely arise from subtle changes in ligand identity or geometry around the Fe center, as would be anticipated for a different pattern of protein sidechain oxygenation in yellow and purple FIH-1.

Oxygenation of Sidechains

Electrospray mass spectrometry was used to identify the protein-derived oxidation products in apo, purple, and yellow FIH-1. FIH-1 samples were digested with trypsin overnight, and then analyzed and sequenced via LC-MS/MS to identify peptides containing active-site aromatics (Tyr^{93}, Tyr^{102}, and Trp^{296}). The Tyr containing peptides, 76 – 99 (MH_2^{2+} = 1387.14 *m/z*) and 100 – 106 (MH^+ = 977.46 m/z) were unmodified in all FIH-1 samples, and the Trp containing peptide 252 – 298 (MH_4^{4+} = 1379.19 m/z) was unmodified in the apo FIH-1 sample. In contrast, both purple and yellow FIH-1 samples contained the unmodified peptide intermixed with an oxygenated peptide (OMH_4^{4+} = 1383.19 m/z) corresponding to a single O-atom addition to peptide 252 – 298 (Figure 9).

High quality MS/MS spectra for yellow and purple FIH-1 samples were obtained by collecting the HPLC fraction containing peptide 252 – 298 for direct injection at 5 μL/min. Scans were averaged to obtain the MS/MS profiles of the unmodified and modified peptides. The site of oxygenation in purple FIH-1 was positively identified as arising from the addition of a single O-atom to Trp^{296} by *b*- and *y*-ion sequencing of this peptide.

Peptide 252 – 298 from yellow FIH-1 was similarly analyzed by direct injection MS/MS using a QStar-TOF. Only limited sequencing was possible, as ions between y_{16} and y_{25} were not observable due to the dominant signal from the y_{25} ion. Nevertheless, oxygenation was localized to the 274 – 283 region, excluding Trp^{296} as the site of oxygenation. As Met oxidation was suspected, collision-induced dissociation (CID) of the infused peptide fraction was performed. The modified y^{25} ion with mass of 1,561.7 *m/z* (*z* = 2+) was selected for MS/MS analysis, and CID was initiated by increasing the declustering potential to 210 V. Fragmentation spectra contained a new peak at 1,529.3 *m/z* (*z* = 2+), corresponding to a total loss of 64 amu from the modified y_{25} (Figure 10). This is characteristic for the loss of a CH_3SOH group from an oxygenated Met residue [44–46], indicating that Met^{275} is the site of oxygenation for yellow FIH-1. In-source CID analysis of purple FIH-1 showed that the only oxygenated residue was Trp^{296}.

While the EPR and XAS data showed similar Fe(III) centers for purple and yellow FIH-1, the MS data indicated distinct peptide modifications. In the case of purple FIH-1, the UV-Vis and MS data together indicated that the oxygenated product was Fe(III)-O-Trp^{296}. Similar Fe(III)-O-Trp chromophores are found in the bacterial enzymes TfdA and AlkB as the products of uncoupled O_2-activation. The indistinct UV-Vis spectrum for yellow FIH-1, on the other hand, indicated an Fe(III) without a new $(Trp/Tyr\text{-}O)^-$ ligand; the MS data indicate that oxygenation occurred, but on a residue (Met^{275}) located at the protein surface, outside of the active site (Figure 1).

This raised the question of whether oxo-Met^{275} and HO-Trp^{296} were mutually exclusive modifications, as for a branched reaction pathway arising from uncoupled oxidation at the active site. Apo FIH-1 (500 μM) was intentionally oxidized at Met residues for 30 min. by excess H_2O_2 (500 mM), followed by the addition of β-mercaptoethanol (1.5 M) [47]. The peroxide-treated apo FIH-1 was split, and one fraction analyzed by MS/MS following trypsin digestion (Figure 11A). The apo FIH-1 sample was quantitatively oxygenated on peptide 252 – 298 (*z* = 4+ peak at 1383.2 *m/z*), as the unmodified peptide (m/z = 1379.2) was not observed.

Subsequent CID experiments on this sample exhibited loss of a CH_3SOH group from the y_{25} ion, confirming that the O-atom addition formed oxo-Met^{275}. The remaining sample of peroxide-treated FIH-1 was used for an auto-hydroxylation assay, which yielded purple FIH-1 (Figure 11B, inset). Trypsin digestion followed by MS/MS analysis indicated that a portion of peptide 252 – 298 was doubly oxygenated (z = 4+ peak at 1387.2 m/z) following auto-hydroxylation, as anticipated for the Fe(III)-O-Trp^{296} chromophore. Clearly, the presence of oxo-Met^{275} does not preclude the formation of Fe(III)-O-Trp^{296} on the same molecule of FIH-1, suggesting that Met^{275} oxidation did not eliminate further active-site chemistry.

Proposed Auto-oxidation mechanism

The consensus chemical mechanism for normal turnover in the αKG oxygenases suggests a mechanism for uncoupled O_2-activation [8]. As the binding of prime substrate releases the axial H_2O from Fe(II), this is the key to making enzyme ready for O_2 binding. Normal turnover leads to the subsequent steps of oxidative decarboxylation, H-atom abstraction, and rebound to produce the hydroxylated product and regenerate resting enzyme. Similarly, inadvertent loss of H_2O prior to prime substrate binding could lead to O_2 activation in the absence of substrate oxygenation. While there are other routes for uncoupling in αKG oxygenases [16,48], the basic theme is one of O_2 entry in the absence of prime substrate.

Our experimental conditions delineated the relationships between multiple enzyme forms, and suggested a role for H_2O-loss in uncoupled O_2-activation by FIH-1 (Scheme 2). Insofar as Co(II) could serve as a structural mimic for Fe(II), the EPR data for (αKG+Co)FIH-1 indicated that Fe(II) within the active site partitioned between a 6C form and a 5C form in which H_2O was likely lost. The mechanistic data were consistent with O_2 binding to the pre-formed αKG-Fe(II) center in resting (αKG+Fe)FIH-1,with a subsequent rate-determining step. Based upon what has been reported for normal turnover in other αKG oxygenases [8,9], the step most likely to be rate-limiting is formation of the Fe(IV)=O intermediate, with subsequent steps leading to Fe(III)-O-Trp^{296}. Yellow FIH-1 arose from a metal centered oxidation in (succ.+Fe)FIH-1 or by the action of glycerol on (αKG+Fe)FIH-1, and contained a fractional (O)Met^{275} modification. It is notable that (O)Met was not observed in the purple FIH-1 samples, implying that purple FIH-1 may be incapable of reacting further with O_2.

It has been proposed that auto-hydroxylation in αKG oxygenases may provide a protective function by inactivating the enzyme to minimize reactive-oxygen species (ROS) production [8], but inactivating an enzyme would also regulate its activity. The potential for auto-hydroxylation to regulate FIH-1 function is intriguing, if for no other reason than it underscores the paradox involved in O_2-sensing by HIFα. As FIH-1 likely functions under physiological conditions in which $[O_2] \gg$ [HIFα], uncoupled oxidation should be common within the cell. Although it would seem energy inefficient to regulate FIH-1 by an irreversible covalent modification, the entire hypoxia-sensing pathway relies on the irreversible hydroxylation of HIFα. Perhaps the resolution lies in kinetics: if auto-hydroxylation were kinetically sluggish, then the ratio of uncoupled turnover to normal turnover would remain small, except for conditions of elevated pO_2. The normal turnover rate for FIH-1 hydroxylating HIFα is already slow ($k_{cat}/K_M = 10^3\ M^{-1}s^{-1}$) [49], but should HIFα be depleted below 10^{-9} M, normal turnover may occur with an observed rate of $<10^{-6}\ s^{-1}$. As purple FIH-1 formation is slightly slower than normal turnover, the relative rates of normal and uncoupled hydroxylation would prevent uncoupling from overwhelming normal turnover, while minimizing aberrant ROS production.

Supplementary Material

Refer to Web version on PubMed Central for supplementary material.

Acknowledgements

We thank the University of Massachusetts, the American Cancer Society (#IRG 93-033) and the NIH (GM077413) for funding; and the NSF for support of the EPR facility (CHE-0443180). We thank Professors S. J. Eyles and R. W. Vachet, and Dr. C. Bobst for helpful suggestions.

Abbreviations

5C, five-coordinate
6C, six-coordinate
AEBSF, 4-(2-aminoethyl)-benzenesulfonyl fluoride
Bis-Tris, 2-[Bis-(2-hydroxyethyl)-amino]-2-hydroxymethyl-propane-1,3-diol
CHES, N-Cyclohexyl-2-aminoethanesulfonic acid
CID, Collision-induced dissociation
ESI-MS, electrospray ionization mass spectrometry
EXAFS, Extended X-Ray Absorption Fine Structure
FIH-1, the factor inhibiting HIF
HEPES, 4-(2-hydroxyethyl)-1-piperazineethanesulfonic acid
HIF, Hypoxia Inducible Factor
IPTG, isopropyl β-D-1-thiogalactopyranoside
MLCT, Metal to Ligand Charge Transfer
Mso, Methionine sulfoxide
ROS, reactive-oxygen species
TOF, Time-of-flight
Tris, 2-Amino-2-hydroxymethyl-propane-1,3-diol
XANES, X-ray Absorption Near Edge Structure
XAS, X-ray absorption spectroscopy
αKG, alpha-ketoglutarate

References

1. Schofield CJ, Ratcliffe PJ. Nat. Rev. Mol. Cell. Bio 2004;5:343–354. [PubMed: 15122348]
2. Semenza GL. Annu. Rev. Cell. Dev. Biol 1999;15:551–578. [PubMed: 10611972]
3. Semenza GL. Physiol 2004;19:176–182.
4. Metzen E, Ratcliffe PJ. J. Biol. Chem 2004;385:223–230.
5. Bruick RK, McKnight SL. Science 2001;294:1337–1340. [PubMed: 11598268]
6. Lando D, Peet DJ, Gorman JJ, Whelan DA, Whitelaw ML, Bruick RK. Gene. Dev 2002;16:1466–1471. [PubMed: 12080085]
7. Mahon PC, Hirota K, Semenza GL. Gene. Dev 2001;15:2675–2686. [PubMed: 11641274]
8. Hausinger RP. Crit. Rev. Biochem. Mol. Biol 2004;39:21–68. [PubMed: 15121720]
9. Price JC, Barr EW, Tirupati B, Bollinger JM, Krebs C. Biochemistry 2003;42:7497–7508. [PubMed: 12809506]
10. Proshlyakov DA, Henshaw TF, Monterosso GR, Ryle MJ, Hausinger RP. J. Am. Chem. Soc 2004;126:1022–1023. [PubMed: 14746461]
11. Zhou J, Gunsior M, Bachmann BO, Townsend CA, Solomon EI. J. Am. Chem. Soc 1998;120:13539–13540.
12. Solomon EI, Brunold TC, Davis MI, Kemsley JN, Lee SK, Lehnert N, Neese F, Skulan AJ, Yang YS, Zhou J. Chem. Rev 2000;100:235–349. [PubMed: 11749238]
13. Zhou J, Kelly WL, Bachmann BO, Gunsior M, Townsend CA, Solomon EI. J. Am. Chem. Soc 2001;123:7388–7398. [PubMed: 11472170]
14. Neidig ML, Brown CD, Light KM, Fujimori DG, Nolan EM, Price JC, Barr EW, Bollinger JM, Krebs C, Walsh CT, Solomon EI. J. Am. Chem. Soc 2007;129:14224–14231. [PubMed: 17967013]
15. Henshaw TF, Feig M, Hausinger RP, Inorg J. Biochem 2004;98:856–861.

16. Koehntop KD, Marimanikkuppam S, Ryle MJ, Hausinger RP, Que L. J. Biol. Inorg. Chem 2006;11:63–72. [PubMed: 16320009]
17. Liu A, Ho RYN, Que LJ, Ryle MJ, Phenney BS, Hausinger RP. J. Am. Chem. Soc 2001;123:5126–5127. [PubMed: 11457355]
18. Saari RE, Hausinger RP. Biochemistry 1998;37:3035–3042. [PubMed: 9485456]
19. Liu PH, Mehn MP, Yan F, Zhao ZB, Que L, Liu HW. J. Am. Chem. Soc 2004;126:10306–10312. [PubMed: 15315444]
20. Sundheim O, Vågbø CB, Bjørås M, Sousa MML, Talstad V, Aas PA, Drabløs F, Krokan HE, Tainer JA, Slupphaug G. EMBO J 2006;25:3389–3397. [PubMed: 16858410]
21. Elkins JM, Hewitson KS, McNeill LA, Seibel JF, Schlemminger I, Pugh CW, Ratcliffe PJ, Schofield CJ. J. Biol. Chem 2003;278:1802–1806. [PubMed: 12446723]
22. Dann CER, Bruick RK, Deisenhofer J. Proc. Natl. Acad. Sci. USA 2002;99:15351–15356. [PubMed: 12432100]
23. Lee C, Kim SJ, Jeong DG, S.M L, Ryu SE. J. Biol. Chem 2003;278:7558–7563. [PubMed: 12482756]
24. Chen Y-H, Comeaux LM, Eyles SJ, Knapp MJ. Chem. Commun. 2008
25. Lennon GG, Auffray C, Polymeropoulos M, Soares MB. Genomics 1996;33:151–152. [PubMed: 8617505]
26. Hewitson KS, McNeill LA, Riordan MV, Tian YM, Bullock AN, Welford RW, Elkins JM, Oldham NJ, Bhattacharya S, Gleadle JM, Ratcliffe PJ, Pugh CW, Schofield CJ. J. Biol. Chem 2002;277:26351–26355. [PubMed: 12042299]
27. Gill SC, von Hippel PH. Anyl. Biochem 1989;182:319–326.
28. Abragam, A.; Bleaney, B. Electron paramagnetic resonance of transition ions. Oxford: Clarendon Press; 1970.
29. Hanson GR, Gates KE, Noble CJ, Griffin M, Mitchell A, Benson S. J. Inorg. Biochem 2004;85:903–916. [PubMed: 15134936]
30. Leitch S, Bradley MJ, Rowe JL, Chivers PT, Maroney MJ. J. Am. Chem. Soc 2007;129:5085–5095. [PubMed: 17397155]
31. Padden KM, Krebs JF, MacBeth CE, Scarrow RC, Borovik AS. J. Am. Chem. Soc 2001;123:1072–1079. [PubMed: 11456660]
32. Ankudinov AL, Ravel B, Rehr JJ, Conradson SD. Phys. Rev. B 1998;58:7565–7576.
33. Bennett B, Holz RC. J. Am. Chem. Soc 1997;119:1923–1933.
34. Bennett B, Holz RC. Biochemistry 1997;36:9837–9846. [PubMed: 9245416]
35. Breece RM, Costello A, Bennett B, Sigdel TK, Matthews ML, Tierney DL, Crowder MW. J. Biol. Chem 2005;280:11074–11081. [PubMed: 15657055]
36. Kumar A, Periyannan GR, Narayanan B, Kittell AW, Kim JJ, Bennett B. Biochem. J 2007;403:527–536. [PubMed: 17238863]
37. Huheey, JE. Inorganic Chemistry: Principles of Structure and Reactivity. Vol. 3rd edn. New York, NY: Harper Collins; 1983.
38. Irving H, Williams RJP. Nature 1948;162:746–747.
39. Irving H, Williams RJP. J. Chem. Soc 1953:3192–3210.
40. Que L, Hausinger RP, Hegg EL, Ho RYN, Liu A, Mehn MP, Ryle MJ. J. Inorg. Biochem 2001;86:388–388.
41. Hegg EL, Whiting AK, Saari RE, McCracken J, Hausinger RP, Que L. Biochemistry 1999;38:16714–16726. [PubMed: 10600135]
42. Pavel EG, Zhou J, Busby RW, Gunsior M, Townsend CA, Solomon EI. J. Am. Chem. Soc 1998;120:743–753.
43. Westre TE, Kennepohl P, DeWitt JG, Hedman B, Hodgson KO, Solomon EI. J. Am. Chem. Soc 1997;119:6297–6314.
44. Jiang XY, Smith JB, Abraham EC. Rapid Commun. Mass Spectrom 1996;31:1309–1310.
45. Lagerwerf FM, vandeWeert M, Heerma W, Haverkamp J. Rapid Commun. Mass Spectrom 1996;10:1905–1910. [PubMed: 9004526]
46. Reid GE, Roberts KD, Kapp EA, Simpson RJ. J. Proteome Res 2004;3:751–759. [PubMed: 15359728]

47. Kim YH, Berry AH, Spencer DS, Stites WE. Protein Eng 2001;14:343–347. [PubMed: 11438757]
48. Ryle MJ, Koehntop KD, Liu AM, Que L, Hausinger RP. Proc. Natl. Acad. Sci. USA 2003;100:3790–3795. [PubMed: 12642663]
49. Ehrismann D, Flashman E, Genn DN, Mathioudakis N, Hewitson KS, Ratcliffe PJ, Schofield CJ. Biochem. J 2007;401:227–234. [PubMed: 16952279]

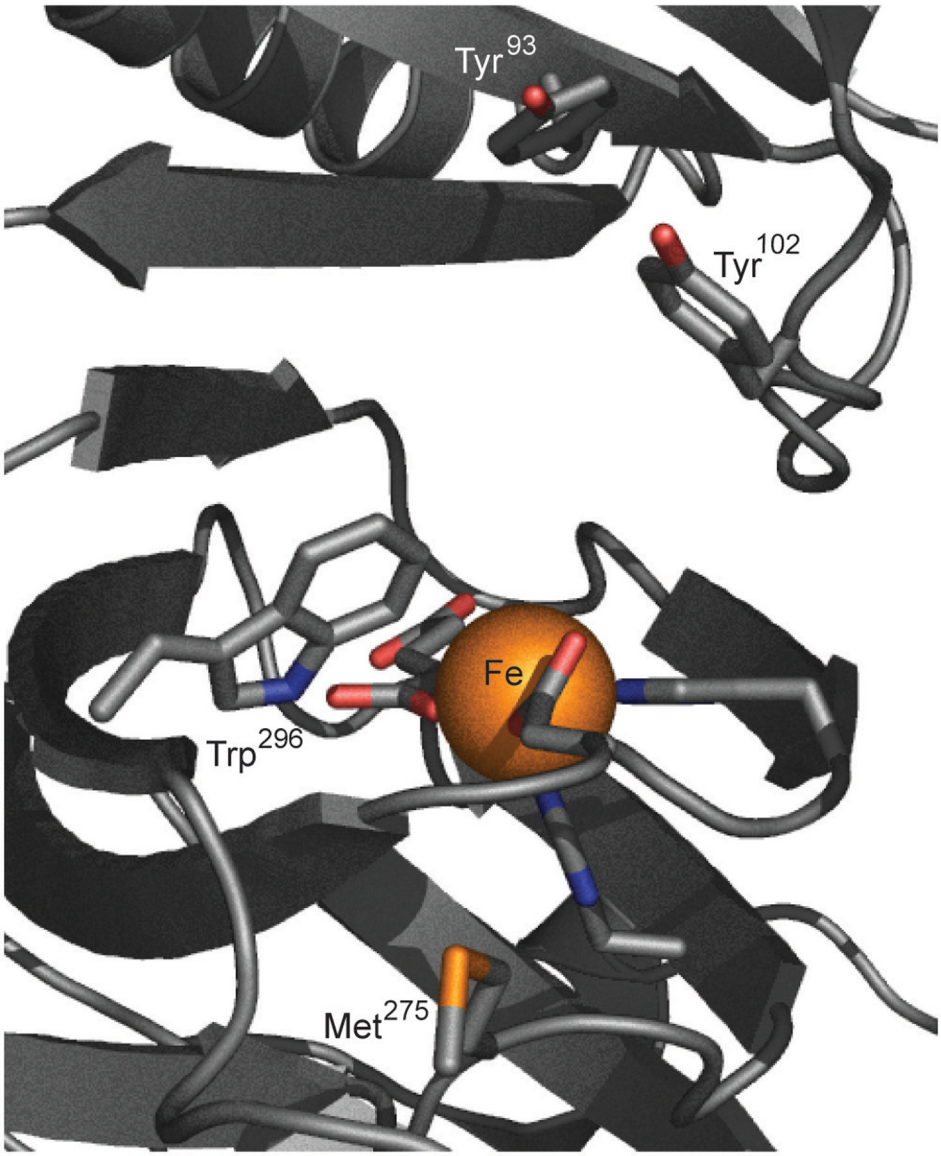

Figure 1.
Active site of human FIH-1 (PDB 1H2K) [21].

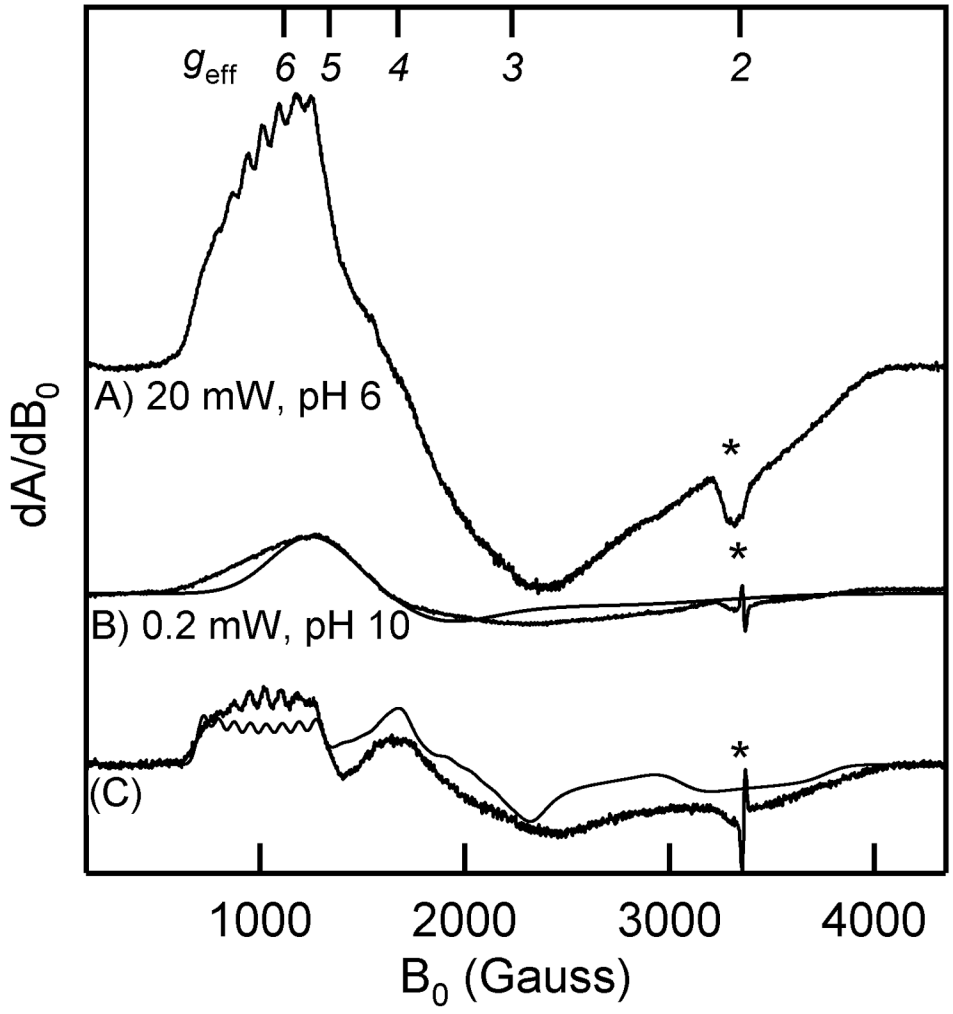

Figure 2.
EPR spectra of (αKG+Co)FIH-1, 10 K, 9.37 GHz, 10 G modulation; A) (αKG+Co)FIH-1 (10 mM Bis-Tris, pH 6.0), 2.0 mW; B) (αKG+Co)FIH-1 (10 mM CHES, pH 10.0), 0.2 mW; Simulation $g_{x,y,z}$ = 2.35 , *E/D* = 0.10; C) Difference spectrum (A–B); Simulation $g_{x,y}$ = 2.60, $g_{x,y}$ = 2.30, *E/D* = 0.23, A = 7.7 mT. * indicates cavity noise.

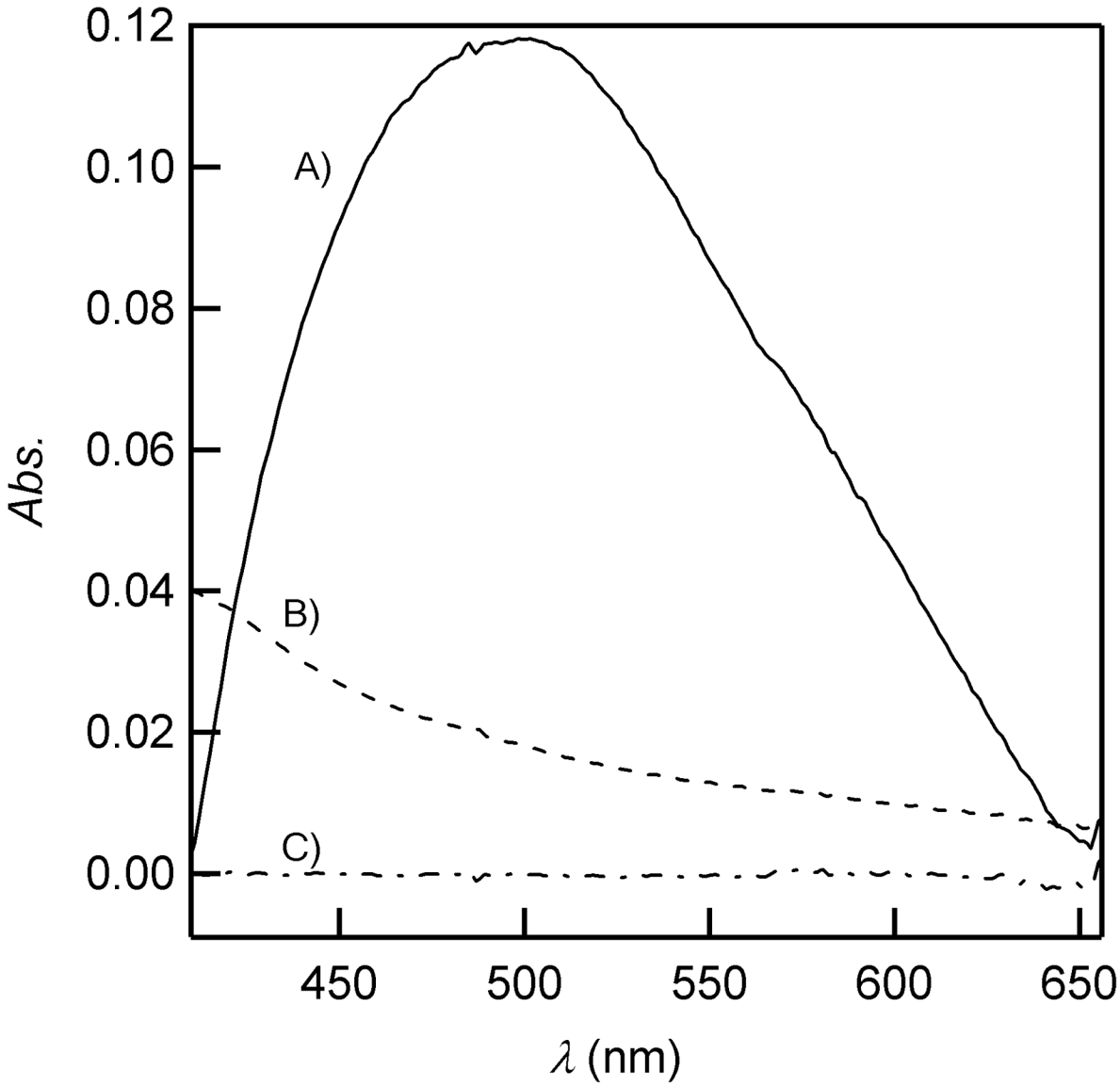

Figure 3.
Difference spectra of resting FIH-1 showing the αKG-Fe(II) MLCT. A) Spectral subtraction of apo FIH-1 from (αKG+Fe)FIH-1 (1.4 mM $FeSO_4$, 1.4 mM αKG); B) Spectral subtraction of apo FIH-1 from (αKG)FIH-1 (1.4 mM αKG); C) Spectral subtraction of apo FIH-1 from a solution of $FeSO_4$ (1.4 mM) and αKG (1.4 mM). All samples 500 μM FIH-1 in 50 mM HEPES, pH 7.50.

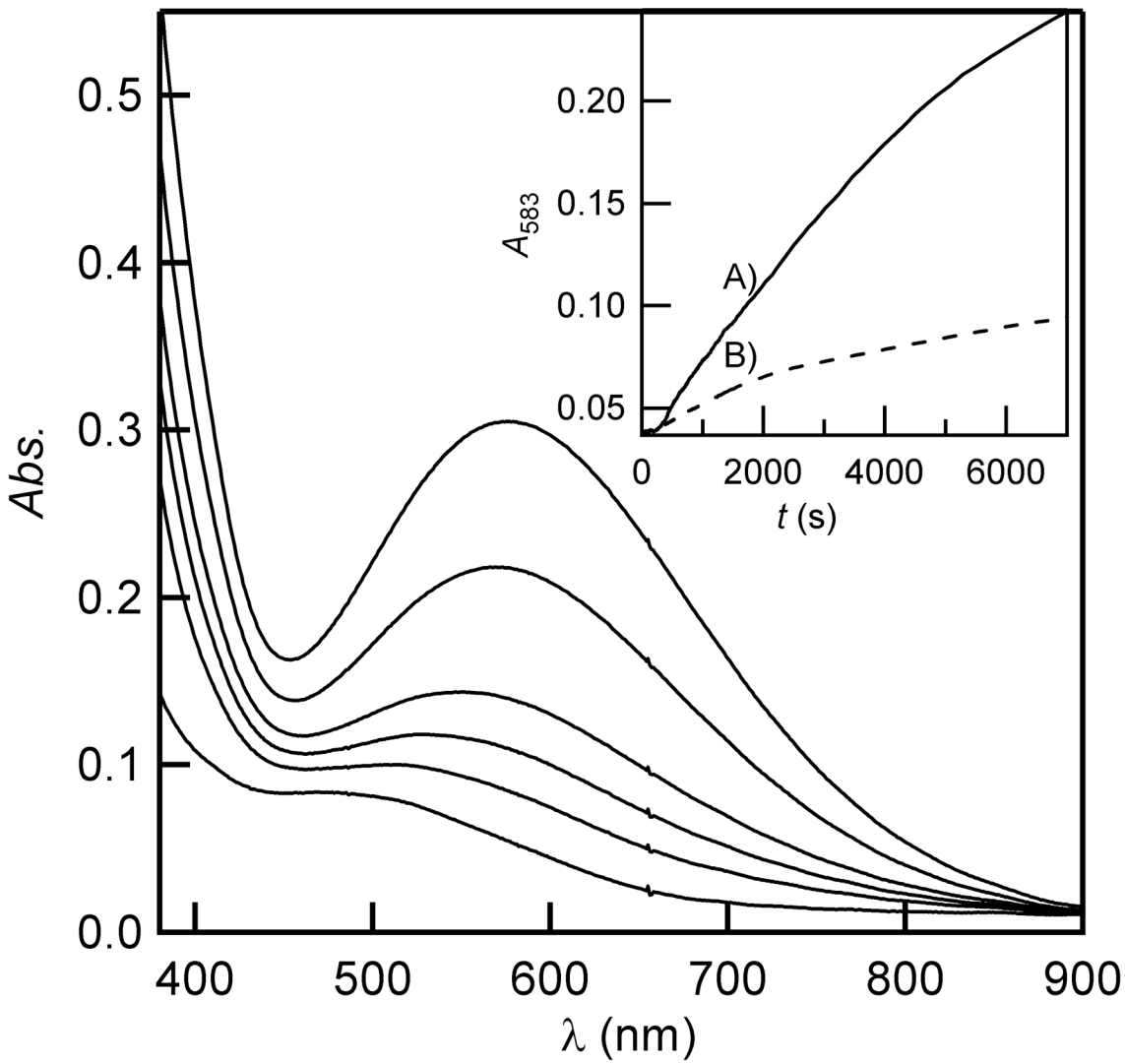

Figure 4.

Appearance of purple FIH-1 following slow exposure of (αKG+Fe)FIH-1 (100 μM apo FIH-1, 500 μM $FeSO_4$, 500 μM αKG in 50 mM HEPES, pH 7.50) to air. Inset: Timecourses following (αKG+Fe)FIH-1 exposure to air; A) slow oxygenation; B) rapid oxygenation.

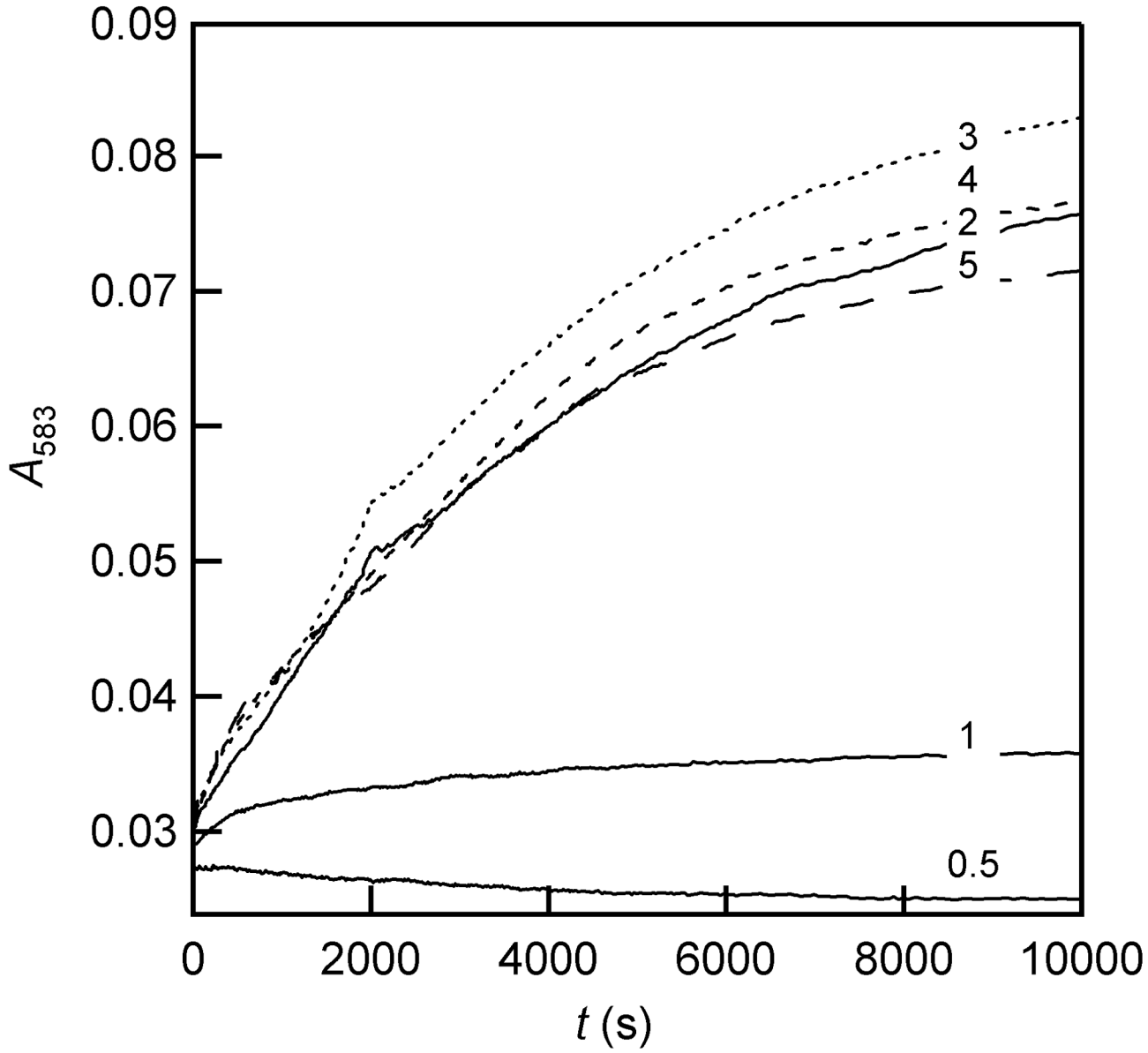

Figure 5.
Kinetics of purple FIH-1 formation following rapid oxygenation of (αKG+Fe)FIH-1 (50 μM apo FIH-1, 25 – 250 μM $FeSO_4$, 250 μM αKG in 50 mM HEPES, pH 7.50). The Fe:FIH-1 ratio is indicated within the figure.

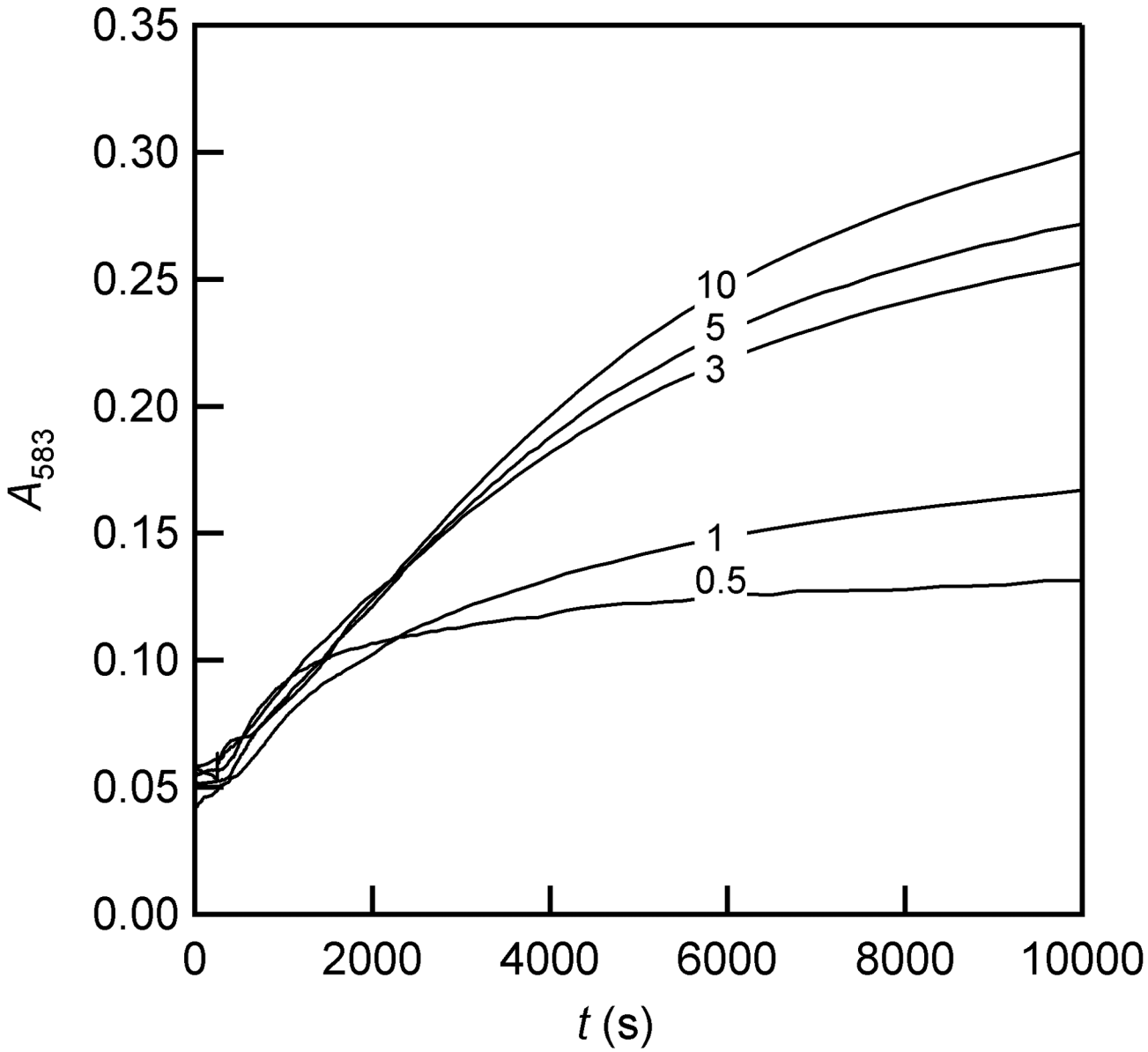

Figure 6.

Kinetic traces (A_{583}) for purple FIH-1 formation following air exposure of (αKG+Fe)FIH-1 (100 μM apo FIH-1, 500 μM $FeSO_4$, 50 – 1000 μM αKG, in 50 mM HEPES, pH 7.50). The αKG:FIH-1 ratio is indicated in the figure.

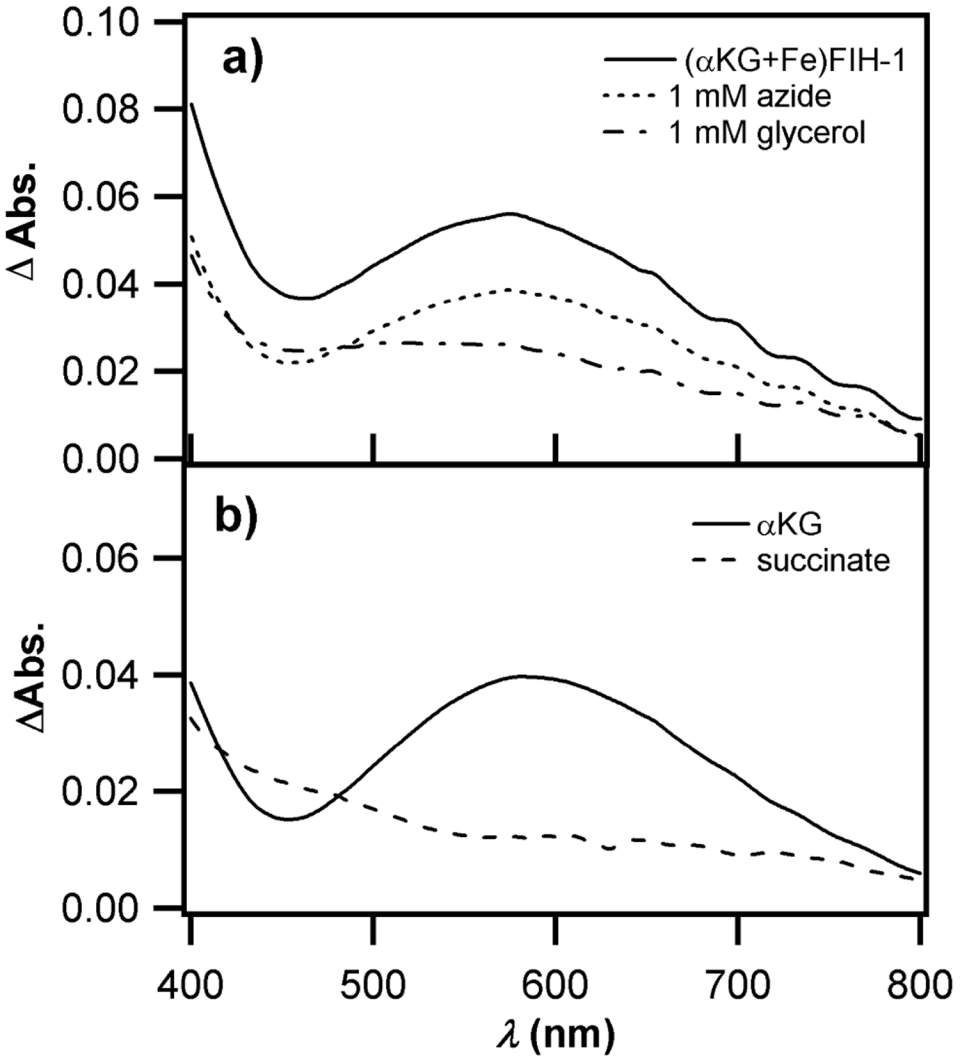

Figure 7.

UV-Vis absorption changes following 10,000 sec. auto-hydroxylation. a) (αKG+Fe)FIH-1 in the presence of A) no additive; B) 1 mM NaN_3; C) 1 mM glycerol. b) 27 Effect of varied organic diacid (αKG/succinate) on auto-hydroxylation, A) (αKG+Fe)FIH-1; B) (succ.+Fe) FIH-1. Conditions: 50 μM FIH-1, 50 μM $FeSO_4$, 250 μM αKG or succinate in 50 mM HEPES, pH 7.50.

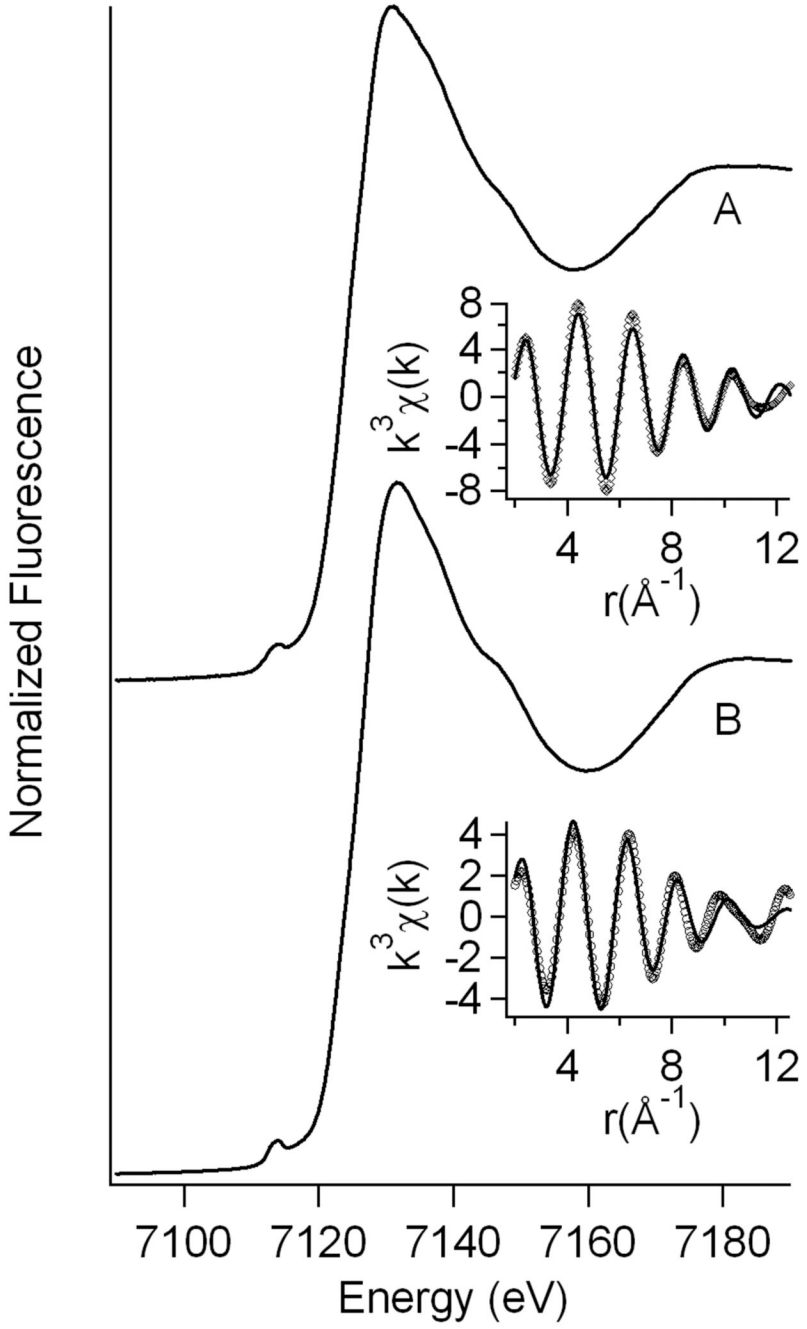

Figure 8.

X-ray absorption spectra; A) yellow FIH-1; B) purple FIH-1. Insets show the Fourier-filtered EXAFS data, and fits using the parameters from Table 1. Samples buffer-exchanged and concentrated from FIH-1 (100 μM in 50 mM HEPES, pH 7.50) with $FeSO_4$ (500 μM) and αKG (500 μM).

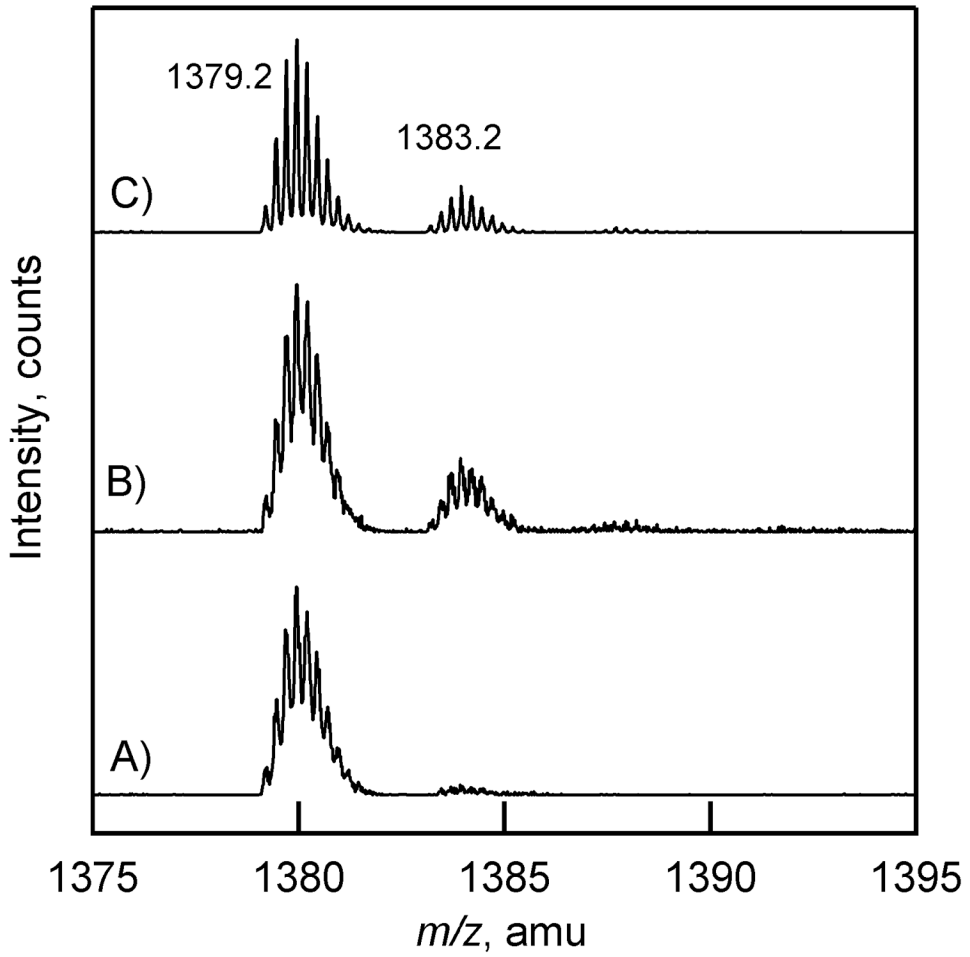

Figure 9.
QSTAR-TOF spectra of peptide 252 – 298 from trypsin digested FIH-1. A) apo FIH-1; B) purple FIH-1; C) yellow FIH-1. The $z = 4+$ peak at $m/z = 1379.2$ is due to unmodified peptide; the $z = 4+$ peak at $m/z = 1383.2$ is due to a singly oxygenated peptide.

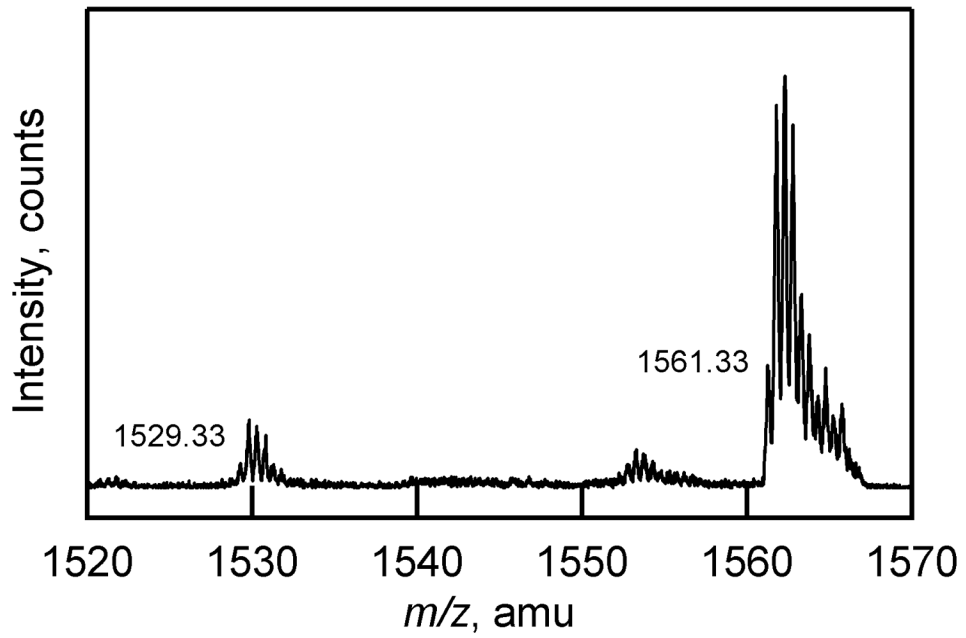

Figure 10.

Fragmentation spectra of y_{25} ion from peptide 252 – 298 of yellow FIH-1 via collision-induced dissociation. The z = 2+ peak at m/z = 1561.3 fragments with loss of 64 mass units to form the z = 2+ peak at m/z = 1529.3.

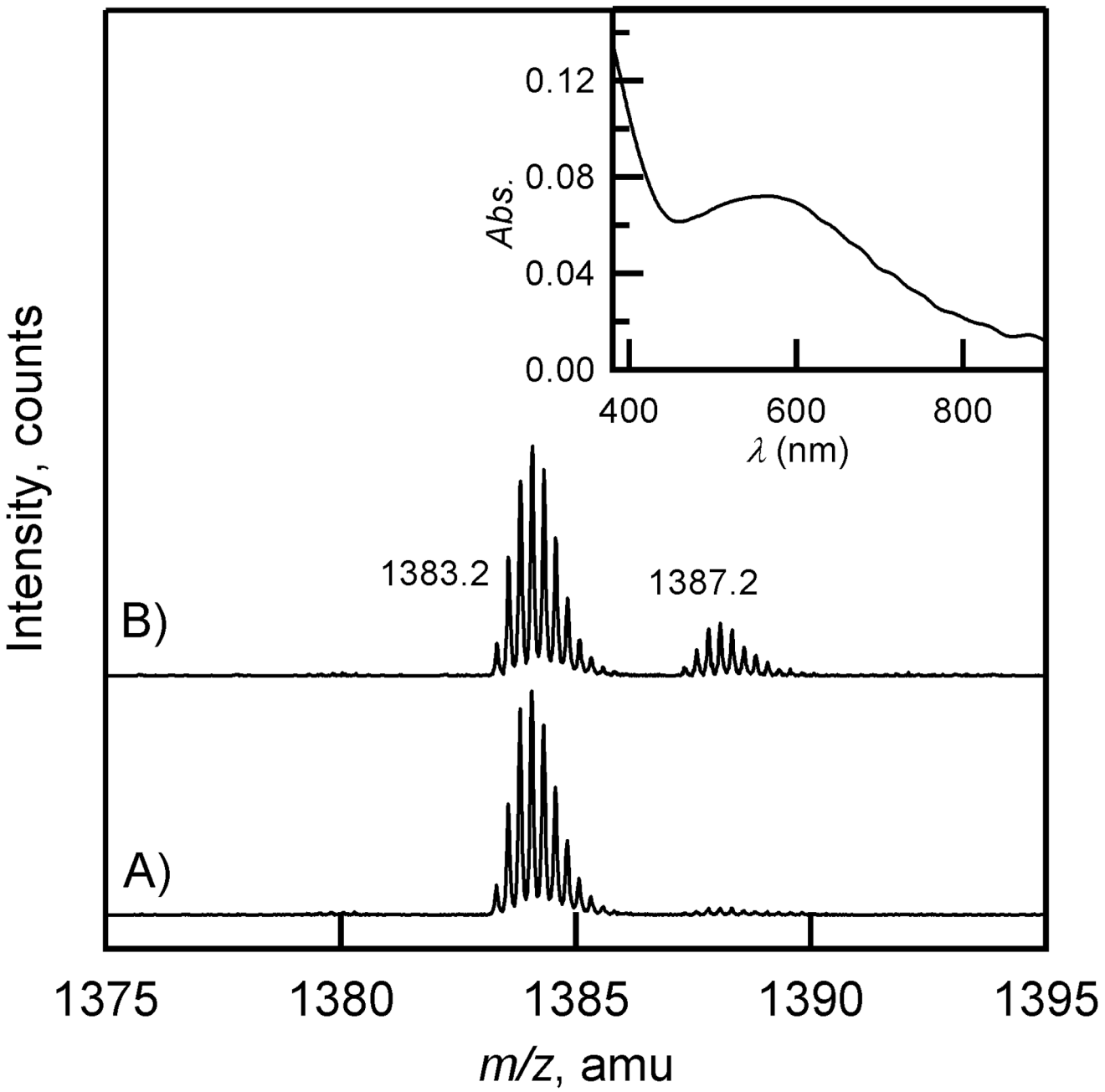

Figure 11.

QStar-TOF spectra of peptide 252 – 298 from H_2O_2-treated FIH-1; A) apo FIH-1; B) (αKG +Fe)FIH-1 following auto-hydroxylation assay. The z = 4+ peaks correspond to peptides that are singly (1383.2 *m/z*) or doubly oxygenated (1387.2 *m/z*). Inset: UV-Vis spectrum of purple FIH-1 formed by rapid oxygenation of peroxide-treated (αKG+Fe)FIH-1 (50 μM apo FIH-1, 50 μM $FeSO_4$, 250 μM αKG in 50 mM HEPES, pH 7.50).

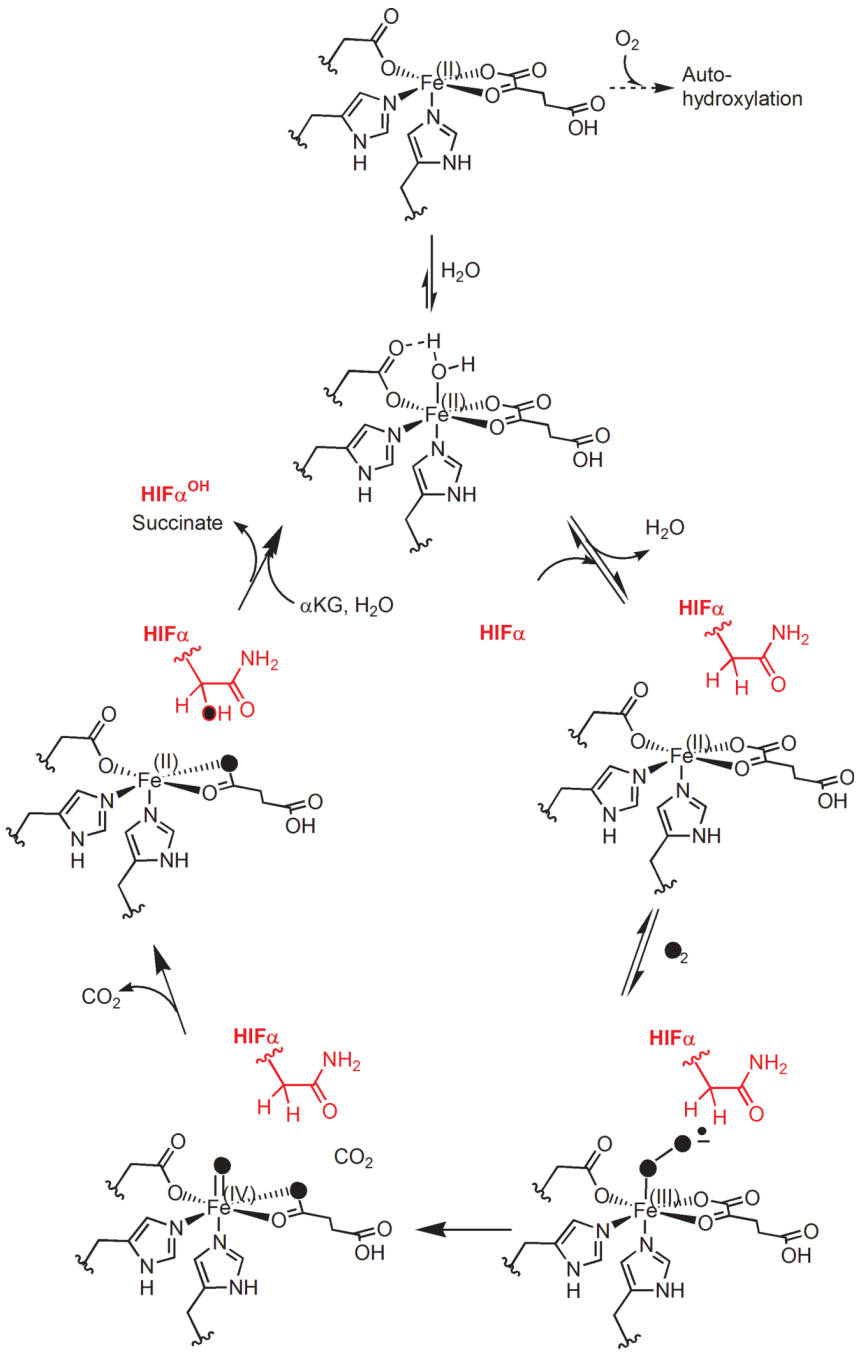

Scheme 1.
Coordination changes at Fe within the consensus mechanism of FIH-1.

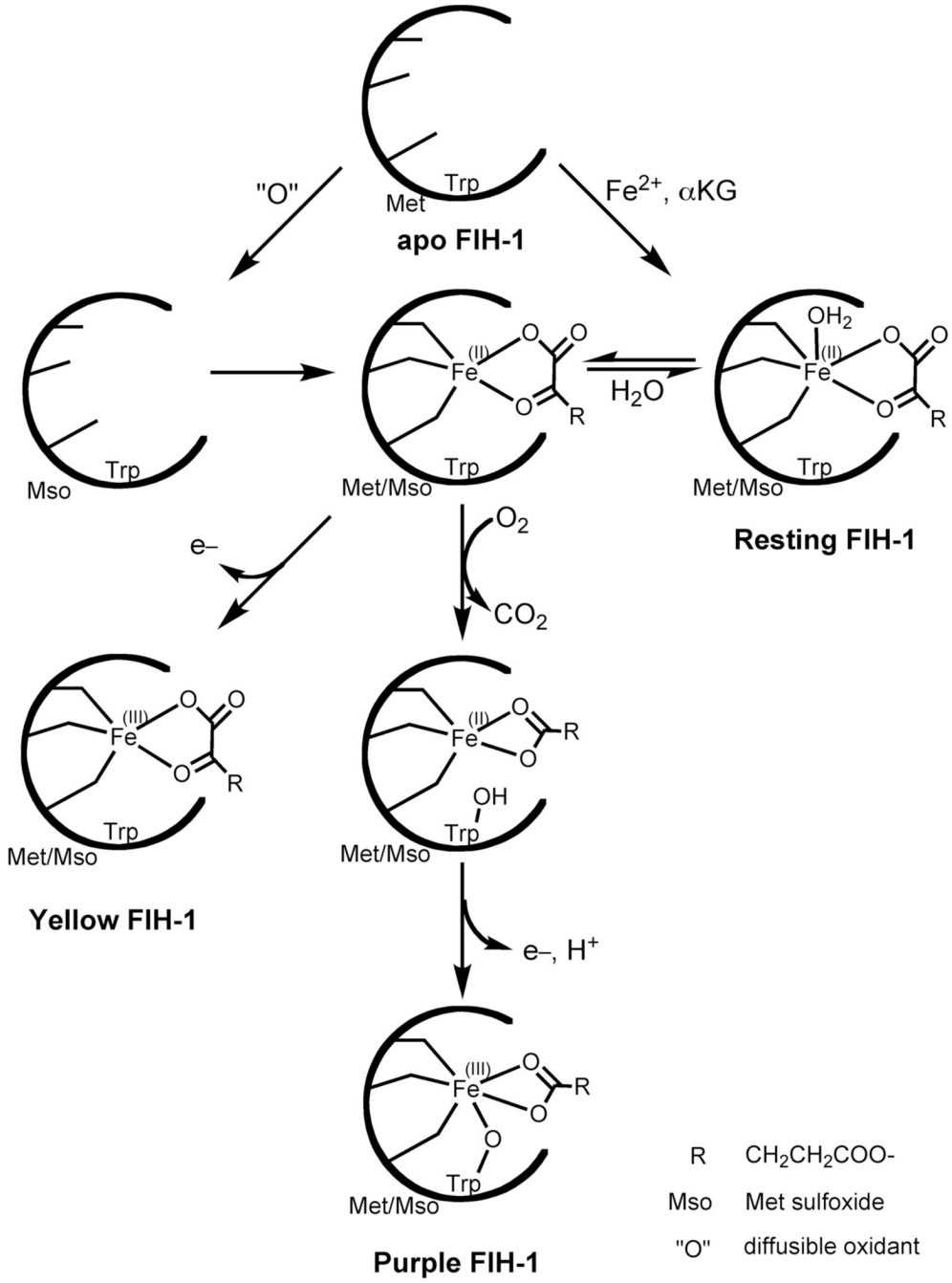

Scheme 2.
Proposed mechanism for converting apo FIH-1 into purple or yellow FIH-1.

Table 1

XAS fits to FIH-1 samples.

Sample	n	r (Å)	σ^2(×10^3 Å^2)	E_0 (eV)	r factor	1s→3d peak area (eV)
Purple	4 N/O 2 N/O	2.11(3) 1.97(4)	6(5) 3(4)	−3(3)	0.0766	0.15(3)
Yellow	7 N/O	2.01(1)	6.5(9)	−2(1)	0.0337	0.12(1)

Best fits reported, with number of first-shell scatterers (*n*), distance to iron (*r*), disorder parameter (σ^2), phase shift (E_0), and the fit *r*-factor. The 1*s* → 3*d* peak area was observed in the pre-edge.